Cloud and Radiation Variations Associated with Northern Midlatitude Low and High Sea Level Pressure Regimes

GEORGE TSELIOUDIS AND YUANCHONG ZHANG

Department of Applied Physics, Columbia University, and
NASA Goddard Institute for Space Studies, New York, New York

WILLIAM B. ROSSOW

NASA Goddard Institute for Space Studies, New York, New York

(Manuscript received 10 November 1998, in final form 23 February 1999)

ABSTRACT

A global meteorological dataset, a global satellite dataset, and a radiative transfer model are combined to map the cloud types in low, near-normal, and high sea level pressure regimes in the northern midlatitudes, and to calculate the radiative balance in those regimes. The prominent cloud feature is a background cloud field that is present most of the time and is modulated by changes in dynamic regime. It consists of a low cloud deck, which becomes optically thicker in the warm seasons over ocean and in the cold seasons over land, and a population of optically thin middle-to-high-top clouds that is mostly middle-top in the cold and mostly high-top in the warm seasons. This background cloud field is modulated by the emergence of a population of optically thick high-top clouds in the low pressure regime and by an increase in the optical thickness of the low clouds in the high pressure regime. The top-of-the-atmosphere (TOA) shortwave flux differences between dynamic regimes show that more sunlight is reflected in the low than in the high pressure regime. In January TOA shortwave flux differences between regimes range between 5 and 20 W m^{-2} and in July between 20 and 50 W m^{-2}, and those differences are manifested as a net excess cooling at the earth's surface. The TOA longwave budget shows more heat trapped in the troposphere in the low pressure than in the high pressure regime. The differences in the TOA outgoing longwave fluxes between the two extreme regimes range in all seasons between 5 and 35 W m^{-2} and are manifested mostly as an additional warming in the atmospheric column. The TOA total flux differences between the low and high pressure regimes change both sign and magnitude with season; in the winter an excess warming of 5–15 W m^{-2} is found in the low pressure regime while in all other seasons an excess cooling, which ranges between 10 and 40 W m^{-2}, is found. Preliminary investigations with the Goddard Institute for Space Studies GCM show that changes in midlatitude dynamics with climate can produce significant radiation feedbacks.

1. Introduction

Comparisons between general circulation model (GCM) simulations of the current climate and satellite-derived radiation fields reveal large errors in the models' top-of-the-atmosphere and surface radiative balance components (Hahmann et al. 1995; DelGenio et al. 1996). The errors are locally of the order 50 W m^{-2} and are of opposite sign in the Tropics and midlatitudes. This implies large errors in the latitudinal gradient of the energy input that drives the poleward energy transports by the atmosphere and the ocean. At a time when climate modelers are attempting to use coupled ocean–atmosphere models to study climate change and variability, such large errors imply significant problems in partitioning energy transport between the atmosphere and ocean, which, in turn, introduces significant uncertainties in the models' present and future climate simulations.

In midlatitude regions, the Goddard Institute for Space Studies (GISS) climate model and the Community Climate Model (CCM2) show excessive amounts of shortwave radiation reaching the surface, resulting in CCM2 summer surface temperature errors over the continents of the order 10°C (Hahmann et al. 1995). Comparisons with cloud data from the International Satellite Cloud Climatology Project (ISCCP) show that the excess amount of incoming solar radiation at the midlatitude surface in the GISS GCM is primarily due to errors in the model-predicted cloud amount and cloud optical properties (DelGenio et al. 1996), which, in turn, are caused either by errors in the moisture transports or by deficiencies in the cloud formation schemes employed

Corresponding author address: Dr. George Tselioudis, NASA Goddard Institution for Space Studies, 2880 Broadway, New York, NY 10025.

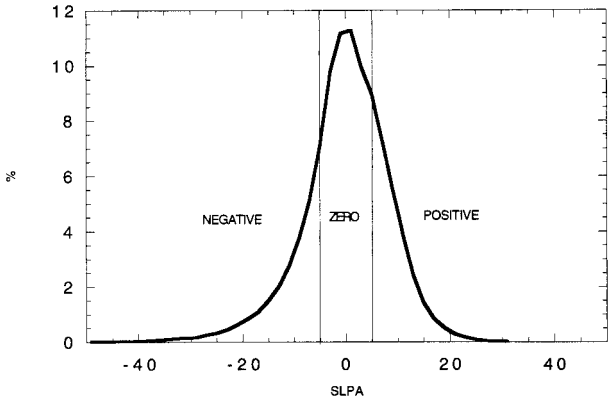

FIG. 1. SLPA frequency histogram and definition of the three (positive, negative, zero) dynamic regimes for Jan 1990 from the NCEP reanalysis dataset.

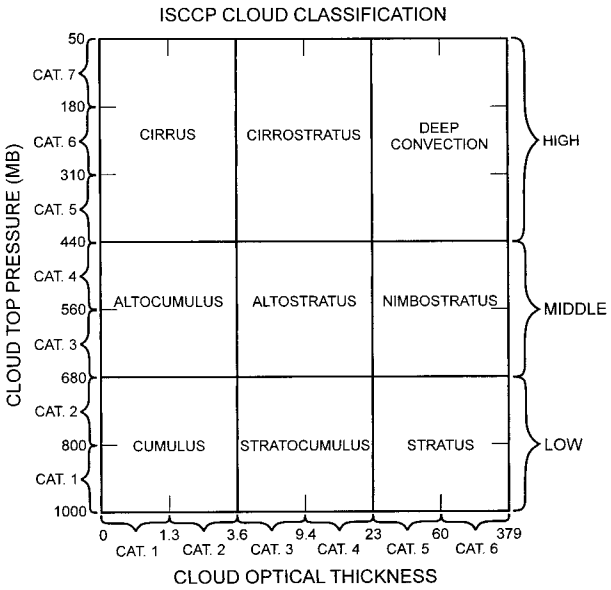

FIG. 2. Definitions of cloud optical thickness and cloud-top pressure categories, together with radiometric definitions of nine cloud types, from the ISCCP D1 dataset.

by the models. Improvement of the representation of extratropical layered clouds in climate models is recognized as an issue of immediate priority and is one of the major goals of the Global Energy and Water Experiment (GEWEX) Cloud System Study (Browning 1994).

Current knowledge of the properties of midlatitude clouds and their relation to the dynamic conditions comes either from qualitative assessments (e.g., Troup and Streten 1972; Evans et al. 1994) or from field studies that examine in detail a limited number of baroclinic storm systems, located usually near mountainous terrain or near the coast with almost no observations over the open oceans or over relatively flat terrain (Ryan 1996). *The synoptic-scale, quantitative relationships between the midlatitude atmospheric dynamics and the properties of the midlatitude clouds are largely unexplored.* Some recent studies that looked at such synoptic-scale relationships between clouds, their radiative effects, and the large-scale atmospheric dynamics are those of Lau and Crane (1995, 1997), who used ISCCP data to explore cloud type distributions in storm track regions of the North and South Atlantic, and Weaver and Ramanathan (1996, 1997), who used Earth Radiation Budget Experiment data to examine the role of extratropical cyclones in determining the cloud radiative forcing over the summertime North Pacific and to relate radiative budget components with large-scale dynamic conditions over the Northern Hemisphere extratropical oceans.

In this study, a global meteorological dataset, a global cloud dataset, and a radiative transfer model are used to examine the differences in cloud properties between different dynamic regimes in the northern midlatitude region, the seasonal variation of those differences, and their effect on the radiative balance of the region. The objective is to map the variations of cloud type with atmospheric dynamic conditions and to quantify the resulting radiative balance changes. This will be done in such a way that the results can be used to evaluate the properties of the midlatitude clouds produced in climate model simulations. Section 2 describes the datasets and radiative transfer model used in this study as well as the method used to analyze the data and initialize the radiative calculations. Section 3 presents the cloud property and radiative budget variations with the large-scale atmospheric dynamics. In section 4 the results of this work are summarized and discussed with emphasis on validation of climate model cloud schemes and on the potential climate feedbacks that the dynamics–cloud–radiation interactions may produce.

2. Datasets and analysis method

a. The NCEP dataset—Definition of dynamic regimes

The National Centers for Environmental Prediction (NCEP) reanalysis grided meteorological dataset is used to define the dynamic regimes used in the subsequent data analysis. It is a global dataset that reports the pressure, temperature, and winds at the surface and at 12 pressure levels in the troposphere. It has a spatial resolution of 2.5° and a time resolution of 12 h. Data for the northern midlatitudes (30°–60°N) in January and July of 1990 are analyzed in this study.

In the first step of the analysis, the NCEP sea level pressure (SLP) values for 1 month are used to separate all 12-hourly observations into three dynamic regimes. First, local monthly mean SLP values are calculated and subtracted from the SLP instantaneous observations, creating 12-hourly sea level pressure anomaly (SLPA) fields. Then, the monthly frequency distribution of all SLPA values in the 30°–60°N region is used to identify the 50th percentile points, that is, the values of SLPA above and below the peak frequency value that divide

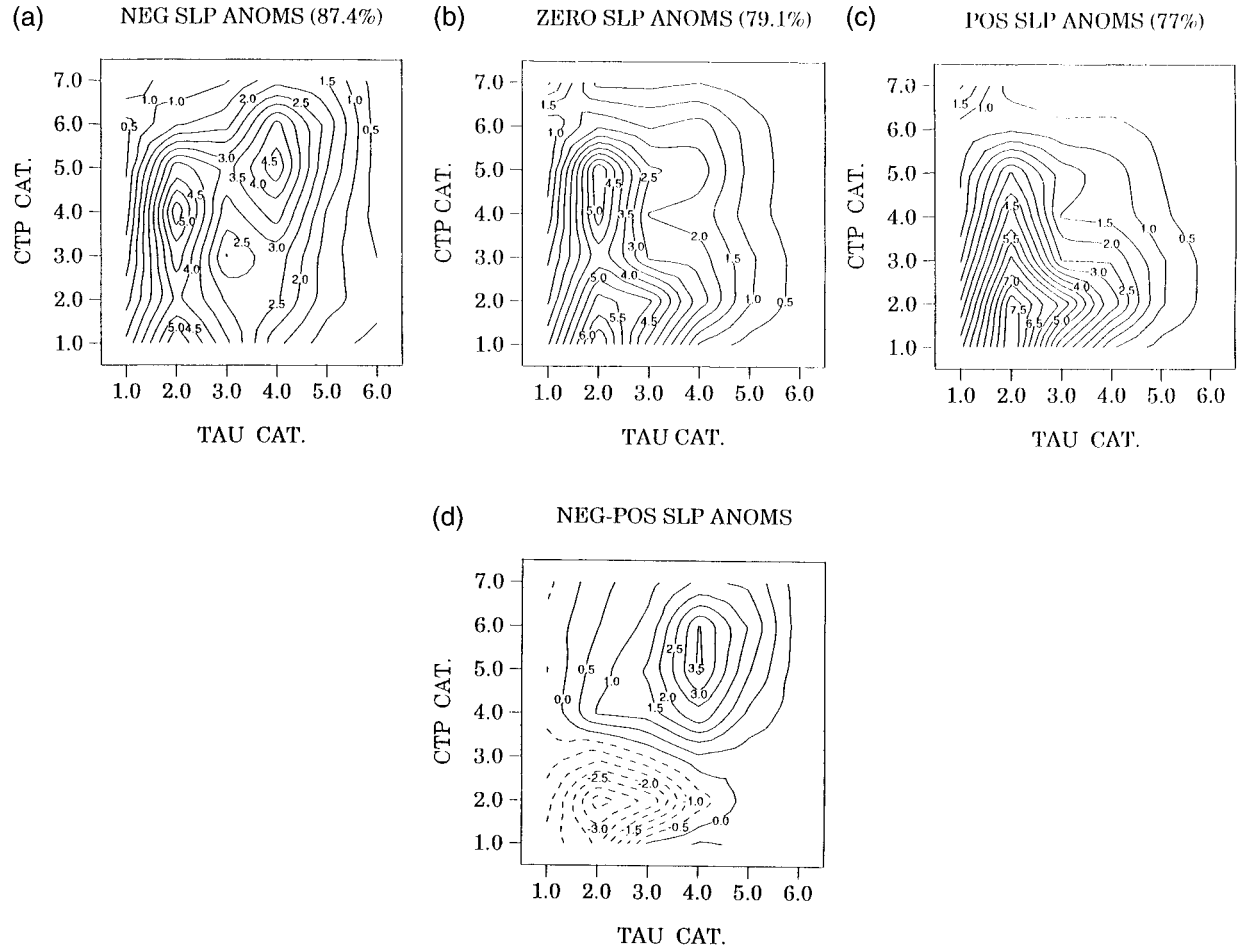

FIG. 3. Distribution of cloud types in the (a) negative, (b) positive, and (c) zero SLPA regimes for clouds over ocean in Jan 1990, along with (d) the difference between the cloud type distributions of the negative and positive SLPA regimes. The points on the *x* and *y* axis represent the TAU and CTP categories defined in Fig. 2. The contours represent the cover by each TAU–CTP type in a regime, with intervals of 0.5%. The total cloud cover for each regime is noted at the top of each plot.

the positive and negative SLPA populations in half. These 50th percentile values define three distinct dynamic regimes: SLPA values lower than the negative 50th percentile point define the ''negative-SLPA'' regime, SLPA values lying between the negative and positive 50th percentile points define the ''zero-SLPA'' regime, and SLPA values higher than the positive 50th percentile point define the ''positive-SLPA'' regime (Fig. 1 illustrates the SLPA frequency histogram and the three regimes for January 1990). The three regimes separate all 12-hourly observations for the month into times of (a) well below average SLP, indicating the passage of a low pressure system; (b) near average SLP, indicating either a dynamically inactive time or a time of transition between low and high pressure systems; and (c) well above average SLP, indicating the passage of a high pressure system.

It is important to note here that in cases when a high pressure system persists in a location for the better part of the month, a negative SLPA may signify the presence of below average high pressure rather than a low pressure system. Since, however, the use of a pressure threshold places in the negative SLPA regime only those SLP values that are much lower than the average value, this exception occurs very infrequently in the analysis. Having noted this caveat, in the rest of the paper we use the terms ''negative/positive SLPA regime'' and ''low/high pressure regime'' interchangeably. Furthermore, the use of the 30°–60°N SLP distribution to identify the 50th percentile points and define the three dynamic regimes produces some latitudinal inhomogeneities, because the variability of the SLP field increases with latitude. As a result, the lower latitudes of the range contribute less than 50% and the higher latitudes more than 50% of values to the positive and negative SLPA regimes. When this regime definition is used to examine results by latitude, the possibility then exists that at particular low latitudes a region with greater SLP variability could dominate zonally averaged quantities derived for the two extreme regimes.

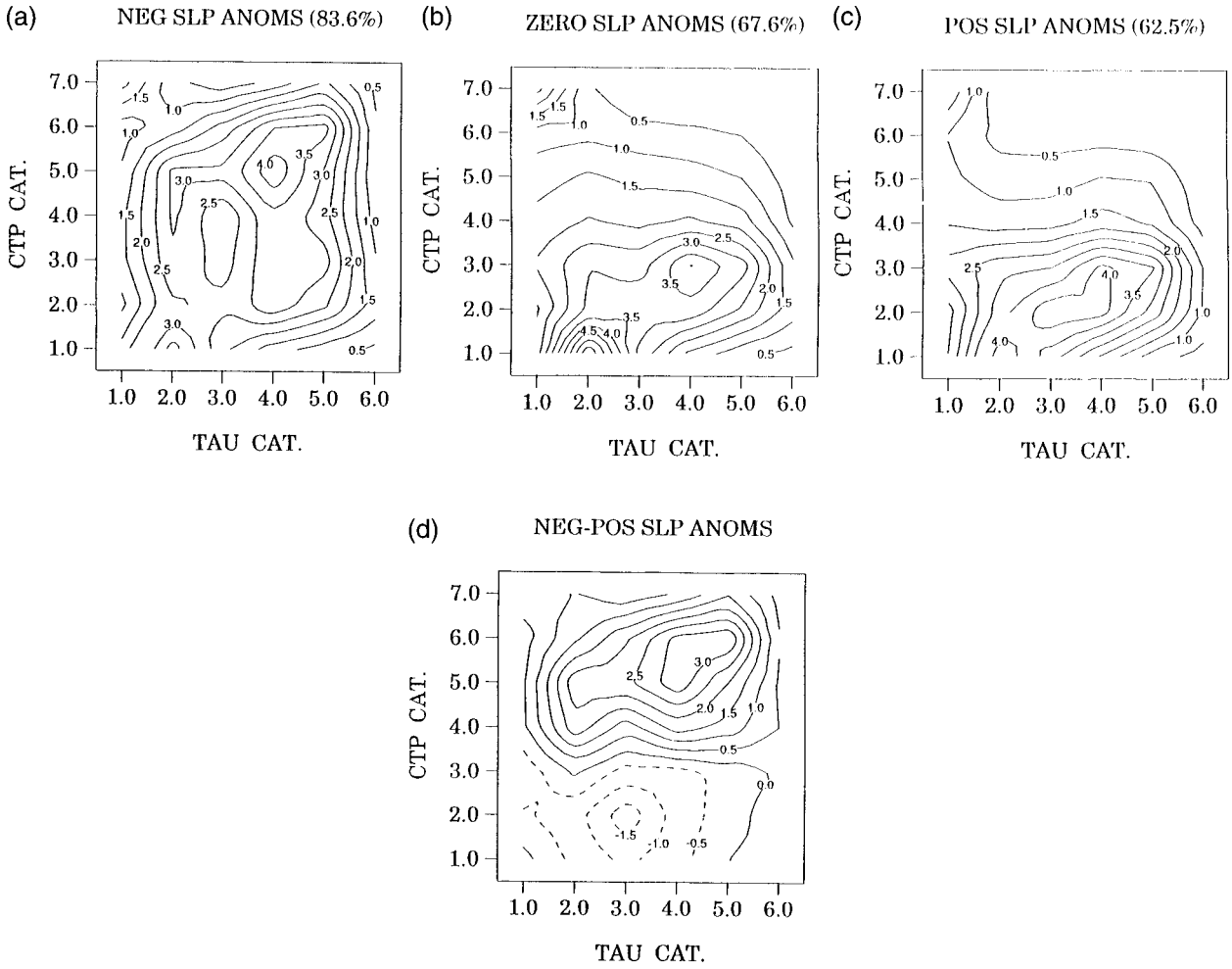

FIG. 4. As in Fig. 3 but for clouds over land.

b. The ISCCP dataset—Construction of cloud-type histograms

The cloud dataset analyzed in this study is produced by the ISCCP (Rossow and Schiffer 1991; Rossow et al. 1996). The dataset contains detailed information on the distribution of cloud radiative properties and their diurnal and seasonal variations, as well as information on the vertical distribution of temperature and humidity in the troposphere. The data are based on observations from the suite of operational weather satellites. The revised (D1) version of the dataset used in this study has a spatial resolution of 280 km (2.5° at the equator) and a temporal resolution of 3 h. For each map grid box, the number of cloudy pixels (approximately 5 km in size) that belong to each of seven pressure levels and six optical thickness ranges is reported. In other words, all cloudy pixels in a grid box are placed in one of 42 cloud optical thickness–cloud-top pressure types. Figure 2 shows the optical thickness ranges and the vertical resolution of the cloud-top pressures, together with radiometric definitions of nine cloud types. A total of 15 cloud types are included in the dataset, since warm low- and midlevel clouds are defined and treated as liquid clouds and cold low- and midlevel clouds are defined and treated as ice clouds.

In the second step of the analysis, the ISCCP retrievals of cloud optical thickness (TAU) and cloud top pressure (CTP) are used to construct TAU–CTP histograms for each corresponding SLPA regime. The histograms are constructed by dividing the TAU–CTP cloud types in each observation with the total cloud cover in the grid box and then calculating for the whole month the percentage of occurrences in each dynamic regime of a cloud of a certain TAU–CTP type. The histograms, then, reveal the cloud types that are dominant during the passage of high pressure systems, low pressure systems, and at times of transition or inactivity. Note that, since cloud optical thickness values are available only during daytime, not all 12-hourly observations in a month are used to construct the TAU–CTP histograms, and that liquid and ice clouds are merged together in each cloud type. From the histograms the total cloud cover in each

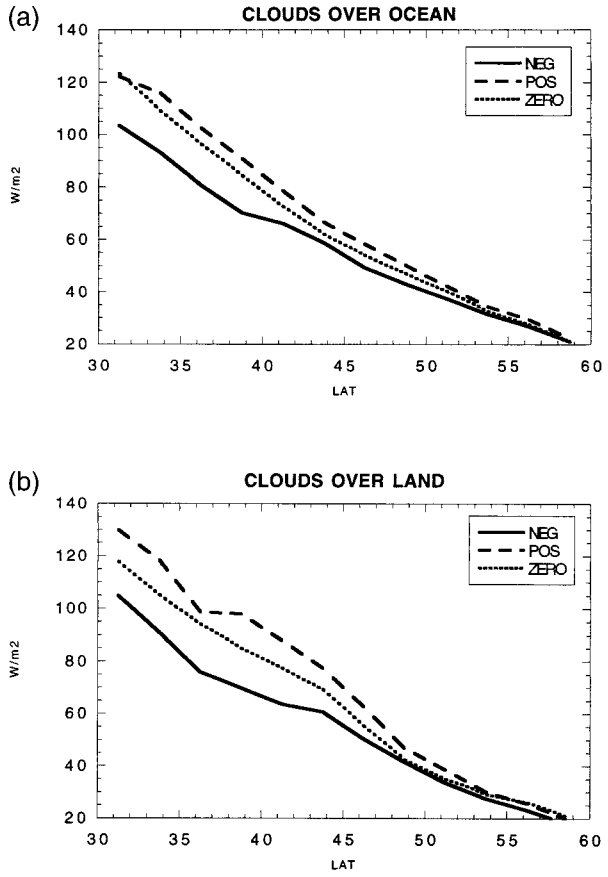

FIG. 5. Latitudinal distributions of the net (incoming minus outgoing) TOA shortwave flux for the negative (solid line), positive (dashed line) and zero (dotted line) SLPA regimes in Jan 1990. Latitude on the *x* axis indicates north latitude.

regime is calculated by adding the cover of all 42 TAU–CTP categories.

c. The radiative transfer model—Calculation of radiation budget components

The radiative transfer model used in this study to compute radiative budget components in the three dynamic regimes is based on the National Aeronautics and Space Administration (NASA) GISS model (Hansen et al. 1983) with some modifications as described in Zhang et al. (1995). The model treats nongray gaseous absorption and thermal emission in a vertically inhomogeneous, multiple-scattering atmosphere and calculates the spectral variation of the upwelling and downwelling shortwave (SW; about 0.2–5.0 μm) and longwave (LW; about 5.0–200.0 μm) fluxes for each atmospheric layer from the top of the atmosphere (TOA) to the surface using the correlated *k*-distribution method (Lacis and Oinas 1991). All significant atmospheric gases are included in the model. Aerosols are based on the climatology mainly from Toon and Pollack (1976) and Charlson et al. (1991). The primary input datasets to the model are ISCCP D1 and D2 datasets (Rossow et al. 1996), including: 1) mean cloud properties (cloud amount, top temperature, and optical thickness), 2) atmospheric temperature and humidity profiles and column ozone amounts from TIROS operational vertical sounder (TOVS), and 3) surface temperature and reflectance. Supplemental datasets for the model include: 1) weekly snow and ice data from the National Oceanic and Atmospheric Administration/National Environmental Satellite Data and Information Service (NOAA/NESDIS) and the Navy–NOAA Joint Ice Center, 2) global land datasets subdivided into eight vegetation types, 3) humidity climatology for pressures $<$300 mb from Oort (1983) and Stratospheric Aerosol and Gas Experiment II (Liao et al. 1995), and 4) a climatology of cloud-layer thicknesses as a function of cloud-top pressure, latitude, and season based on rawinsonde and surface observations (Wang and Rossow 1995).

The prominent features of the model are that all the radiatively important physical properties of the atmosphere, clouds, and surface are separate inputs, so that their radiative effects may easily be diagnosed, and that the calculated fluxes from TOA to surface are self-consistent. Furthermore, the use of the model allows us to derive radiative fluxes consistent with the cloud-type distributions that we derive in step 2 of the analysis. From the validation study by Rossow and Zhang (1995), the uncertainties of the model using ISCCP C1 data for regional, monthly mean fluxes are about 5–15 W m^{-2} and 10–20 W m^{-2} for TOA and surface, respectively.

In the third step of the analysis, the definition of dynamic regimes from step 1 is used to derive regime cloud property distributions (similar to those in step 2) and vertical profiles of temperature and humidity; those distributions and profiles are then used as input to the radiative model in order to calculate the components of the radiative budget in each of the three dynamic regimes. The results determine the radiative budget differences between strong high pressure systems, strong low pressure systems, and periods of near-normal sea level pressure. To use the model for this study, we have made the following modifications. 1) The input temperature and humidity profiles are now monthly and 2.5° zonal means, calculated separately for land and ocean and for the three dynamic regimes as described above. 2) All the ancillary datasets, including snow–ice and Oort–SAGE datasets, are also averaged into monthly and zonal means in this fashion. 3) Cosine solar zenith angle is averaged to such monthly and zonal means. 4) All clouds are treated as liquid water clouds, reducing the maximum number of cloud types from 15 to 9. Since the ISCCP D1 dataset retrieves the properties of colder clouds using an ice microphysical model and since an ice cloud with the same optical thickness has a $\sim$10% (relative) larger albedo than a water cloud (Mishchenko et al. 1996), our treatment will introduce a small but systematic underestimate of cloud albedo for higher level and higher latitude clouds relative to lower level and

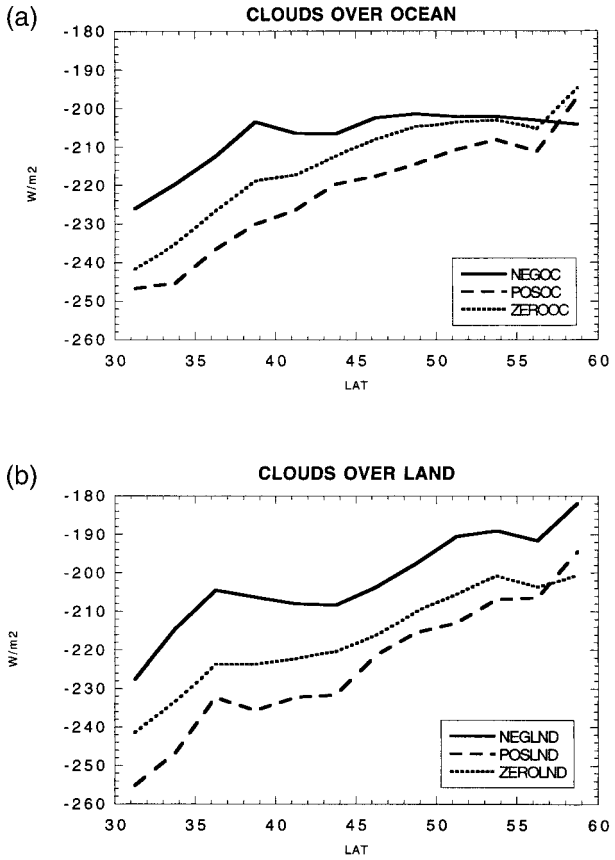

FIG. 6. As in Fig. 5 for the net TOA longwave flux.

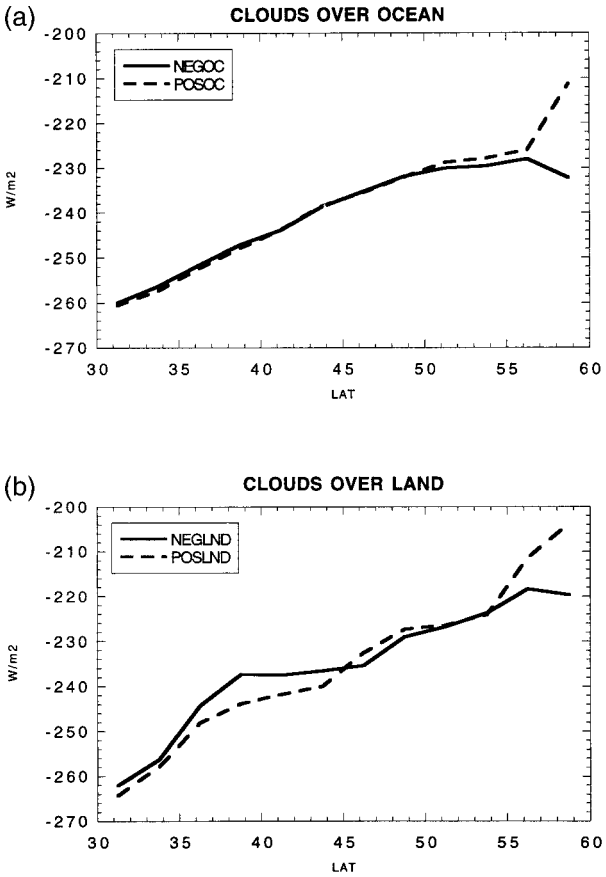

FIG. 7. Latitudinal distributions of the net clear-sky TOA longwave flux for the negative (solid line) and positive (dashed line) SLPA regimes in Jan 1990. Latitude on the *x* axis indicates north latitude.

lower latitude clouds. 5) Clear sky is defined by the same vertical atmospheric profile as for the mean cloudy conditions except mean cloud optical thickness is set to zero. 6) The full-sky fluxes are then obtained by weighting the cloudy fluxes of the nine cloud types using their corresponding cloud fractions and the clear-sky flux with its fraction within a latitudinal zone.

3. Results

Data for January and July of 1990 are analyzed to derive the cloud-type distributions and radiative balance components in low pressure, high pressure, and near-normal pressure regimes. The analysis is done for the Northern Hemisphere midlatitude region (30°–60°N) separately over land and ocean, and results are presented below for the 2 months.

a. January 1990

The distribution of cloud types in the negative, positive, and zero SLPA regimes for ocean clouds in January 1990 are shown in Figs. 3a–c, along with the difference between the cloud type distributions of the negative and positive SLPA regimes (bottom). The contours on the plots represent the cover by each TAU–CTP type in a regime with intervals of 0.5%. The total cloud cover for each regime is noted at the top of each plot. The cloud amounts are very high in all three regimes; the lowest cloud cover observed occurs in the positive SLPA regime (77%). The difference in cloud cover between negative and positive SLPA regimes is only 10.4%. A background cloud field of optically thin, low-, and middle-top clouds dominates all three dynamic regimes. The low pressure regime includes an additional population of optically thick, high-top clouds, while in the high pressure regime the low-cloud peak extends into the middle optical thickness category. Cloud types in the zero SLPA regime are intermediate between the positive and the negative SLPA regimes, roughly depicting the structure of the background cloud field.

The cloud type distributions in the three dynamic regimes over wintertime continental regions are plotted in Fig. 4. They show cloud amounts that are smaller overall than over oceans but are still high in all dynamic regimes; again the lowest cloud cover occurs in the positive SLPA regime (62.5%). The difference between the cloud cover of high and low pressure areas is much larger than for oceanic clouds (21.1%). The background cloud field contains mostly middle optical thickness,

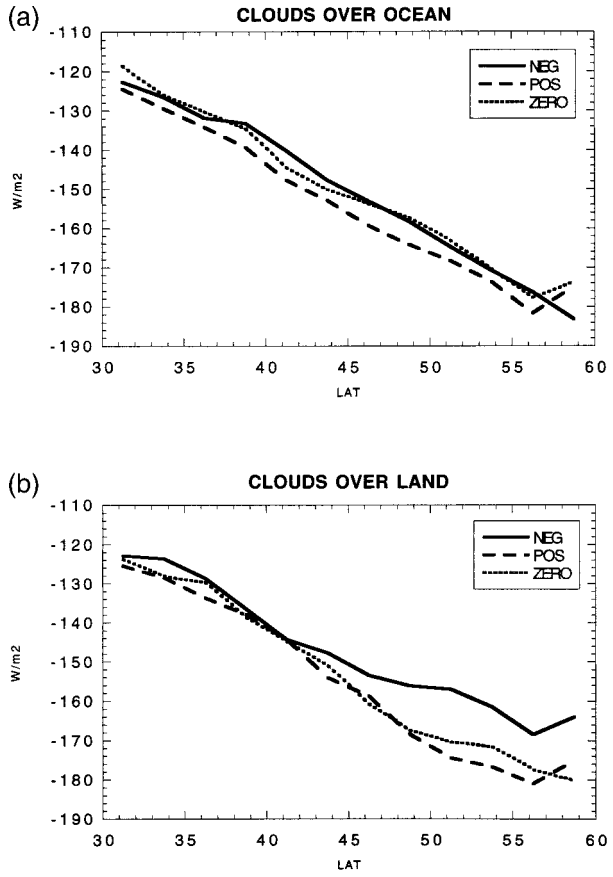

FIG. 8. As in Fig. 5 for the net total (shortwave plus longwave) TOA flux.

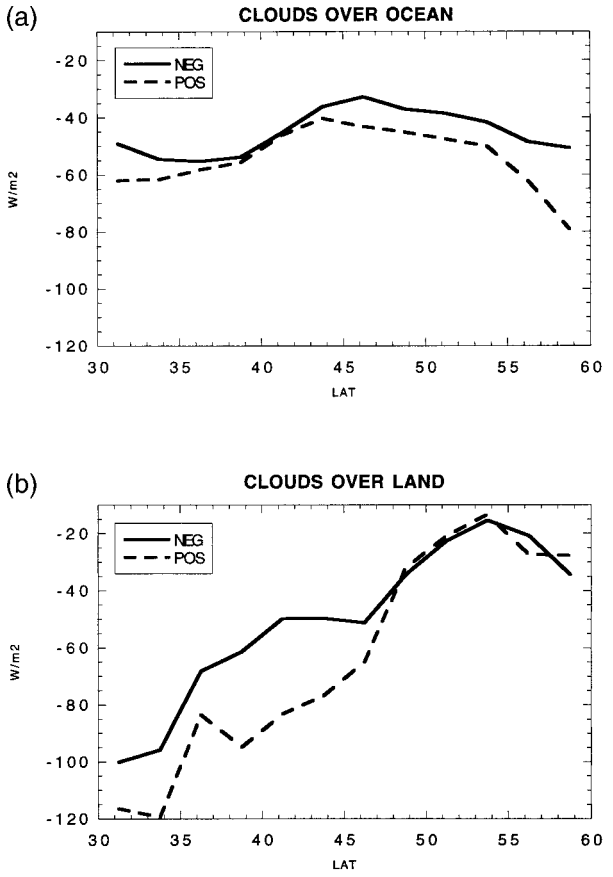

FIG. 9. As in Fig. 7 for the net surface longwave flux.

low- with some middle-top clouds with a second peak in the low-top optically thin cloud category. This background low cloud field becomes optically thicker in the zero and positive SLPA regimes while in the negative SLPA regime a new peak occurs in the optically thick, high-top cloud category. The difference plots for oceanic (Fig. 3d) and continental (Fig. 4d) clouds show that the high-to-low SLP transition is associated with a low-thin-to-high-thick cloud transition.

The latitudinal distributions of the net TOA shortwave flux for the three regimes in January 1990 are shown in Fig. 5. Both over ocean (Fig. 5a) and over land (Fig. 5b) more sunlight is reflected by the clouds in the low pressure than in the high pressure regime, consistent with the higher cloud cover and optical thicknesses of clouds in the negative SLPA regime (Figs. 3 and 4). The flux difference between negative and positive SLPA regimes ranges from 10–20 W m^{-2} south of 45°N to 0–10 W m^{-2} north of 45°N as wintertime solar insolation decreases with latitude. This difference is somewhat larger over continental regions, where values reach up to 30 W m^{-2}, due to the fact that cloud cover differences between the two regimes are more pronounced over land than over ocean. The fluxes in the zero SLPA regime fall between the two other regimes, somewhat closer to the positive one.

The latitudinal distributions of the TOA longwave fluxes for the three regimes in January 1990 are shown in Fig. 6. Both over ocean and over land, less heat escapes into space in the negative than in the positive SLPA regime and the flux difference between the regimes ranges between 0 and 30 W m^{-2} over ocean and between 10 and 35 W m^{-2} over land. Longwave flux differences between the regimes can be due either to cloud type and cover differences or to differences in the temperature and humidity profiles of the atmospheric column. To distinguish between the two, the clear-sky fluxes are compared for the two extreme regimes. The clear-sky TOA longwave flux differences between the negative and positive SLPA regimes are shown in Fig. 7, over ocean (a) and over land (b). The fluxes for the two regimes differ very little, implying that the differences observed in the total flux (Fig. 6) are mostly due to the higher thicker cloud tops in the negative SLPA regime (Figs. 3d and 4d).

The latitudinal distributions of the total net TOA flux for the two regimes in January 1990 are shown in Fig. 8. Both over ocean and over land, longwave flux differences between the regimes dominate the shortwave

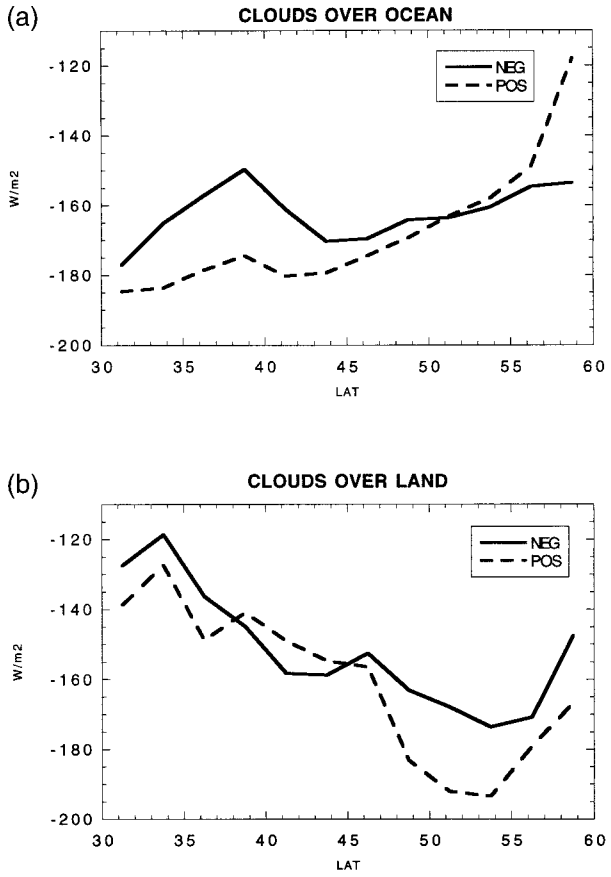

FIG. 10. As in Fig. 7 for the net in-atmosphere longwave flux.

ones, producing a smaller cooling of the atmospheric column in low pressure than in high pressure regions. This cooling reduction ranges between 2 and 6 W m^{-2} in maritime regions and is as large as 20 W m^{-2} for continental regions in the latitude zone between 50° and 55°N.

The TOA radiative balance is indicative of the cloud effects on the planetary radiative budget. To clarify which part of the earth–atmosphere system is actually affected by the cloud differences between low and high SLP regimes, the surface and in-atmosphere radiative budget components are also calculated (the in-atmosphere component is calculated as the difference between the surface and TOA components). The surface net shortwave flux (not shown here) show differences between the three regimes that are identical to the ones observed in the TOA flux (Fig. 5). This indicates that the additional shortwave reflectance observed in the negative SLPA regime is manifested as a cooling at the surface and has little effect on the in-atmosphere radiative balance.

The surface longwave fluxes for the negative and positive SLPA regimes are shown in Fig. 9, separately over ocean (a) and over land (b). While the ocean fluxes show only small differences between the regimes south of 45°N and larger differences of the order 10 W m^{-2} north of 45°N, the land fluxes exhibit the opposite behavior with large differences of the order 20 W m^{-2} south of 45°N and no flux differences between the two regimes north of 45°N. When compared to the TOA longwave differences between the regimes (Fig. 6), these differences imply that south of 45°N over ocean and north of 45°N over land the additional warming in the low pressure regions is realized mostly in the atmospheric column and has little effect on the surface radiative balance, while north of 45°N over ocean and south of 45°N over land the warming is realized almost entirely at the surface. This is more clearly illustrated in Fig. 10, where the in-atmosphere longwave flux differences between the two regimes are shown for maritime (a) and continental clouds (b).

b. July 1990

The distribution of cloud types in negative, positive, and zero SLPA regimes for ocean clouds in July 1990 are shown in Figs. 11a–c, along with the difference in the distributions between the negative and positive SLPA regimes (Fig. 10d). The cloud amounts in all three regimes are very high, with the lowest cloud cover occurring in the zero SLPA regime (70.8%) and with the difference in cloud cover between the positive and negative SLPA regimes at 11.1%, similar in magnitude to the difference found in January. In all three regimes, the background cloud field is dominated by medium optical thickness, low-top clouds (the July background low clouds are thicker than the January ones), with a secondary peak in the optically thin, high-top cloud category (these clouds are higher than in January). In the negative SLPA regime an additional peak of optically thick, high-top clouds appears that is smaller in magnitude than the one found in the January observations. Cloud types in the zero SLPA category are again representative of the structure of the background cloud field. The difference plot between the positive and negative SLPA regimes reveals a transition from low-top moderately thick to high-top optically thick clouds.

The distribution of summertime continental cloud types between the three regimes for July 1990 is shown in Fig. 12. The lowest cloud cover occurs in the positive SLPA regime (59.7%), and the difference in cloud cover between positive and negative SLPA regimes is 14.2%, smaller in magnitude than the difference observed in wintertime clouds. The cloud field in all three regimes is dominated by a background of optically thin, high clouds with a secondary population of thin low clouds (much thinner than the low clouds observed in January). In the positive SLPA regime the low cloud deck becomes somewhat thicker while in the negative SLPA regime an additional peak is found in the optically thick, high-top cloud category, a peak that is smaller than the one found in the January observations. The difference plot between negative and positive SLPA regimes (Fig.

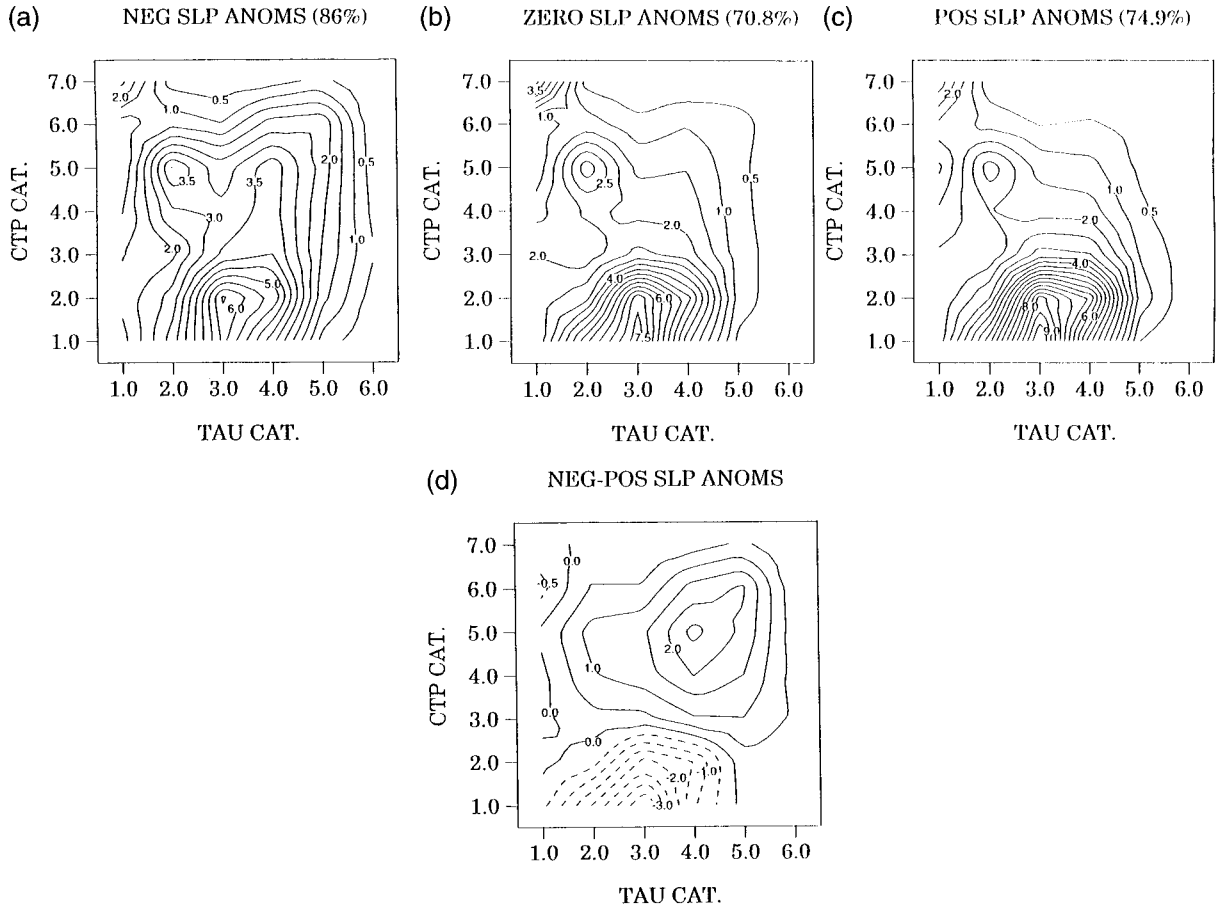

FIG. 11. Distribution of cloud types in the (a) negative, (b) positive, and (c) zero SLPA regimes for clouds over ocean in Jul 1990, along with the difference between the cloud type distributions of the negative and positive SLPA regimes (bottom). The points on the *x* and *y* axes represent the TAU and CTP categories defined in Fig. 2. The contours represent the cover by each TAU–CTP type in a regime, with intervals of 0.5%. The total cloud cover for each regime is noted at the top of each plot.

12d) shows greater cloud amounts in almost all cloud types in the low SLP regions, with the exception of high cirrus clouds that are more abundant in high SLP regions.

The latitudinal distributions of the net TOA shortwave flux for the three regimes in July 1990 are shown in Fig. 13. Over ocean (Fig. 13a) significantly more solar radiation is reflected in the negative SLPA regimes. The flux differences between the two extreme regimes range from 20 to 50 W m^{-2} (larger in part because of a higher average sun position in summertime) and are largest in the extreme northern and southern latitudes of the range. Over land, south of 40°N only small differences between the fluxes in the three regimes are observed, with the positive regime reflecting 5–15 W m^{-2} more sunlight than the negative one. North of 40°N, however, more sunlight is reflected in the negative regime; the flux difference between the regimes increases going northward and reaches 50 W m^{-2} in latitudes north of 50°N. The net surface shortwave flux differences between regimes (results not shown here) are almost identical to the TOA ones, implying that the additional cooling in the low pressure areas is manifested at the surface.

The latitudinal distributions of the net TOA longwave flux for the three regimes in July 1990 are shown in Fig. 14. Both over land and ocean more thermal radiation is emitted into space in the positive SLPA regime, with the exception of continental regions south of 40°N. The differences in the outgoing longwave flux between the two extreme regimes range between 5 and 25 W m^{-2}. When the TOA clear-sky longwave fluxes are plotted (Fig. 15), very small differences between the regimes are found, indicating that the excess heat trapped in the low pressure regime is due to the higher tops of the clouds (Figs. 11d and 12d). The exception again is continental regions south of 40°N, where even under clear-sky conditions more heat is emitted into space in the low than in the high pressure regions.

To understand how the TOA longwave fluxes are partitioned between the surface and the atmosphere, the net surface longwave fluxes for the three regimes are plotted in Fig. 16. In most areas the flux differences between

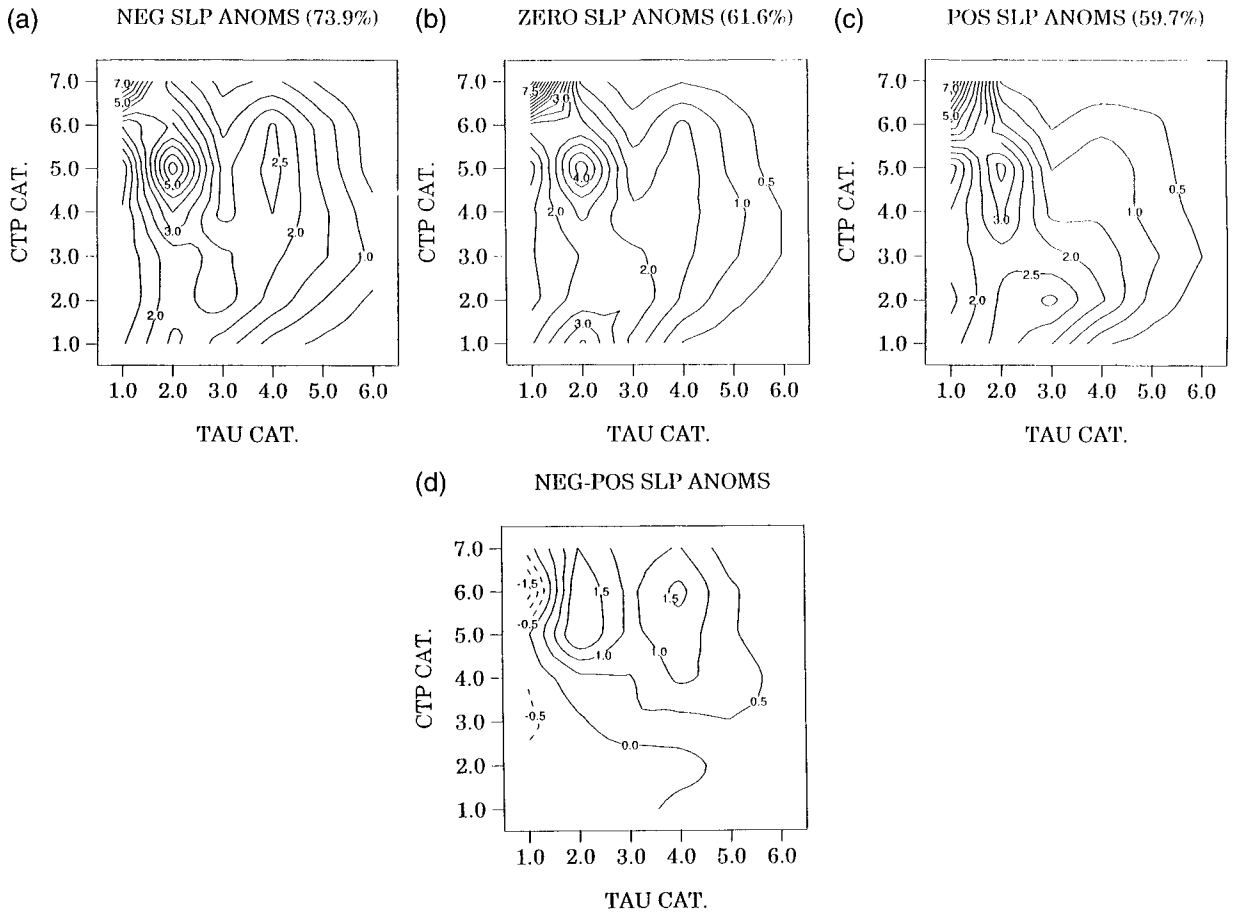

FIG. 12. As in Fig. 11 but for clouds over land.

regimes are very small, indicating that most of the additional longwave heating of the low pressure regions observed in the TOA budget (Fig. 14) is manifested in the atmosphere and has only a small effect at the surface. The exceptions once again are continental regions south of 40°N, where much more heat is emitted from the surface in the low than in the high pressure regime.

The continental band between 30°N and 40°N contains primarily desert regions and the Tibetan Plateau. To investigate how those two regions contribute to the zonally averaged longwave fluxes in the three dynamic regimes, the separate SLPA distributions for those regions were examined. The results show that in this particular July the SLPA values had a much greater variance in the Tibetan Plateau than in the deserts, particularly on the positive side of the distribution. As a result, the positive SLPA statistics are dominated by grid points located over the Tibetan Plateau. Since the surface temperature of the plateau is a lot smaller than in the deserts, the average positive SLPA regime emits less thermal radiation at the surface than the negative and zero SLPA regimes.

The summertime differences of the net TOA total fluxes between regimes (Fig. 17) are dominated by the shortwave flux differences (Fig. 13), which are almost everywhere larger than the longwave flux differences (Fig. 14). As a result, an additional cooling is observed in the low pressure regions that ranges between 10 and 40 W m^{-2}. Exception again are continental regions south of 40°N where the differences in the net total TOA fluxes between regimes are very small.

Analysis of data from April and October 1990 showed results that were closer to the ones found in the July than in the January data. An example is shown in Fig. 18, where the net total TOA fluxes for the three regimes in April 1990 are plotted. An additional cooling is observed in the low pressure regions that, as in July, varies in magnitude between 10 and 40 W m^{-2}. Note that the anomalous behavior over land regions south of 40°N is present only in the analysis of the July data. Analysis of data from 4 months in 1987 showed results similar to the ones found for 1990.

4. Summary and discussion

A global meteorological dataset, a global satellite dataset, and a radiative transfer model were combined to map the cloud properties in low, near-normal, and high

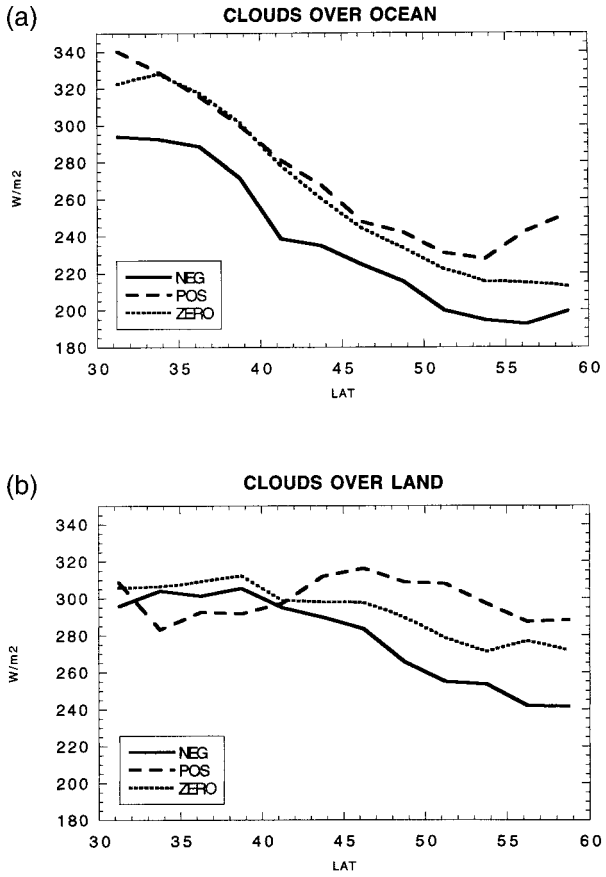

FIG. 13. Latitudinal distributions of the net (incoming minus outgoing) TOA shortwave flux for the negative (solid line), positive (dashed line), and zero (dotted line) SLPA regimes in Jul 1990. Latitude on the *x* axis indicates north latitude.

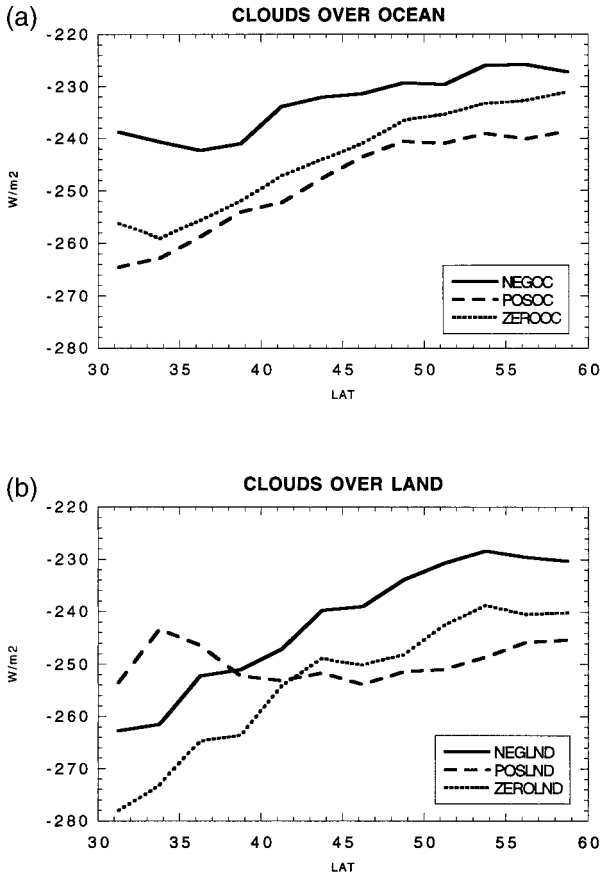

FIG. 14. As in Fig. 13 but for the net TOA longwave flux.

SLP regimes, and to calculate the radiative balance in those three regimes. The prominent cloud feature in the northern midlatitude atmosphere is a background cloud field that is present most of the time and is only modulated by changes in the atmospheric dynamic regime. This is in agreement with the results of Lau and Crane (1995), who looked at time series of cloud optical thickness in the North Atlantic and found episodes of large optical thickness superimposed on a background of low optical thickness. The predominance of the background cloud field is particularly true over oceans, where cloud amounts in all regimes are consistently higher than 70% and the cloud cover differences between low and high SLP regimes do not exceed 12%. The background cloud field over oceans consists of a low cloud population, which increases in optical thickness in the high pressure regime, and a population of optically thin middle-to-high-top clouds that are somewhat more abundant in the negative SLPA regime. This background field is augmented by a population of optically thick high-top clouds in the low pressure regime. Seasonal comparisons over oceans show that the background low cloud population is optically thicker in July than in January, the thin middle-to-high clouds are fewer and somewhat higher in July, and the optically thick high-top cloud peak in the negative SLPA regime is more pronounced in January. In continental regions, the differences in cloud cover between low and high SLP regimes are larger than over oceans, reaching values as large as 21% in January. Over the continents, the background cloud field generally consists of a low cloud population and a population of optically thin high-top clouds, but this picture is seasonally dependent since in January the low cloud population is a lot larger and optically thicker than in July while in July, the optically thin high-top clouds are more abundant than in January. The background field is modified by the addition of an optically thick high-top cloud peak in the low SLP regime that is more pronounced in January than in July, and by an increase in the optical thickness of the low clouds in the positive SLPA regime. In all seasons, the cloud types in the zero SLPA regime are intermediate between the two extreme regimes and represent fairly closely the structure of the background cloud field.

The January maritime cloud type changes with dynamic regime can be compared to the study of Lau and Crane (1995), even though their study concentrated only on the strongest storm events (as defined by the exis-

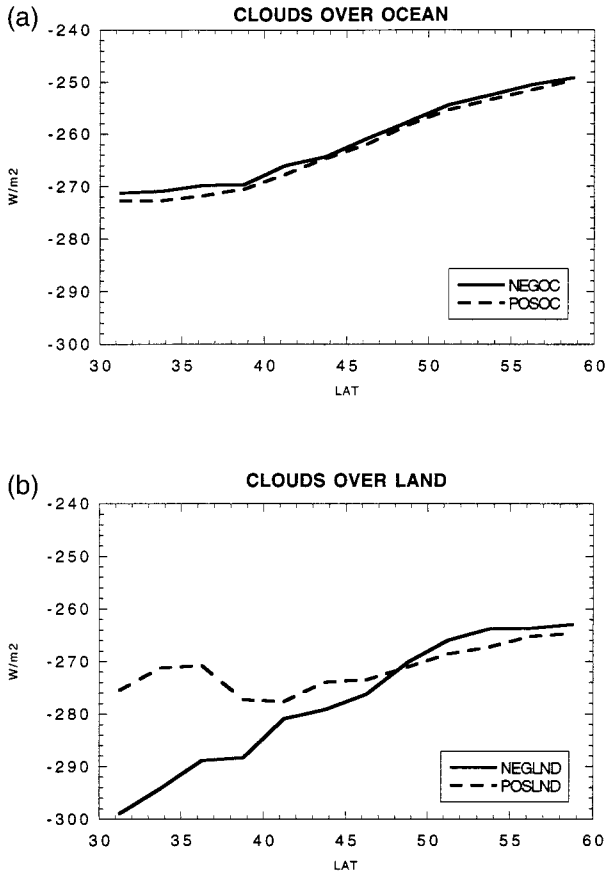

FIG. 15. Latitudinal distributions of the net clear-sky TOA shortwave flux for the negative (solid line) and positive (dashed line) SLPA regimes in Jul 1990. Latitude on the *x* axis indicates north latitude.

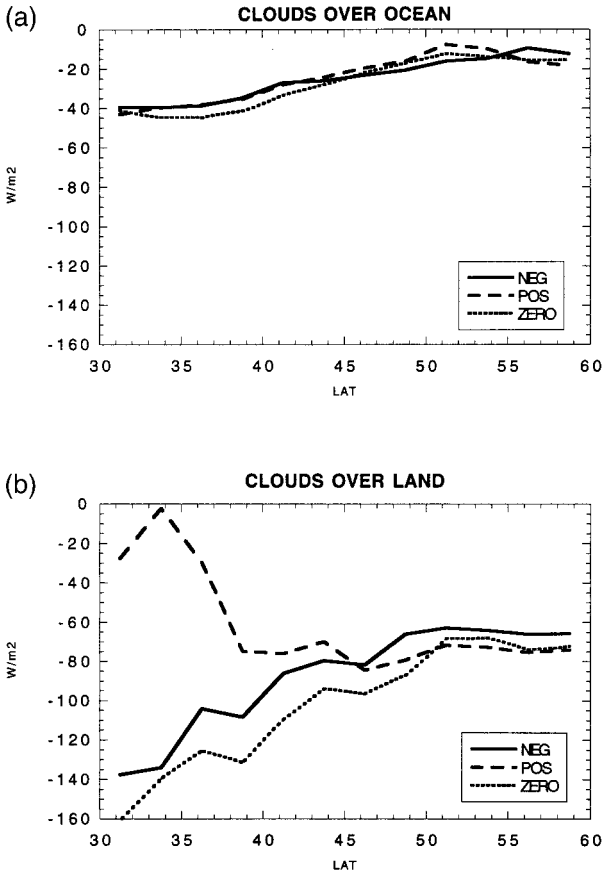

FIG. 16. As in Fig. 13 but for the net surface longwave flux.

tence of extremely optically thick clouds) while ours incorporates all observed events in one of the three SLPA regimes. Even though qualitative agreement exists between the two studies in terms of the progression from low-thin to high-thick clouds between the positive and negative SLPA regimes, the results of Lau and Crane (1995) show that in strong storms the high-thick cloud deck intrudes into the high pressure regime, and that other dynamic fields such as vertical velocity or temperature advection may better isolate the distinct cloud types present in intense storm systems. Sea level pressure is a reliable and simple parameter that was used here to derive a first look at the relations between cloud type distributions and dynamic regime and that makes simple the comparison of our results with GCM simulations. The use of alternative definitions of dynamic regime, using combinations of atmospheric fields, will make easier the examination of the atmospheric processes responsible for the cloud type changes and will be the subject of future work.

The differences in the shortwave fluxes between dynamic regimes show that more sunlight is reflected in the low than in the high SLP regime, due to the larger cloud cover and optical thicknesses. The magnitude of the TOA shortwave flux differences between the two regimes, however, is highly dependent on the available solar insolation and, therefore, the season; in January those differences range only between 5 and 20 W m^{-2}, while in July they range between 20 and 50 W m^{-2} depending on latitude and underlying surface. These TOA flux differences are manifested as a net excess cooling at the earth's surface and have little effect on the in-atmosphere radiative balance. The TOA longwave budget shows more heat trapped in the troposphere in the low pressure than in the high pressure regime. The differences in the outgoing longwave fluxes between the two extreme regimes range in all seasons between 5 and 35 W m^{-2}. This excess heat is manifested mostly as an additional warming in the atmospheric column and has little effect on the surface radiative budget. When both the longwave and shortwave components are combined the resulting TOA total flux differences between the negative and positive SLPA regimes change both sign and magnitude with season; in the winter an excess warming of 5–15 W m^{-2} is found in the negative SLPA regime, while in all other seasons an excess cooling, which ranges between 10 and 40 W m^{-2}, is found.

The seasonal differences in the effect of dynamic re-

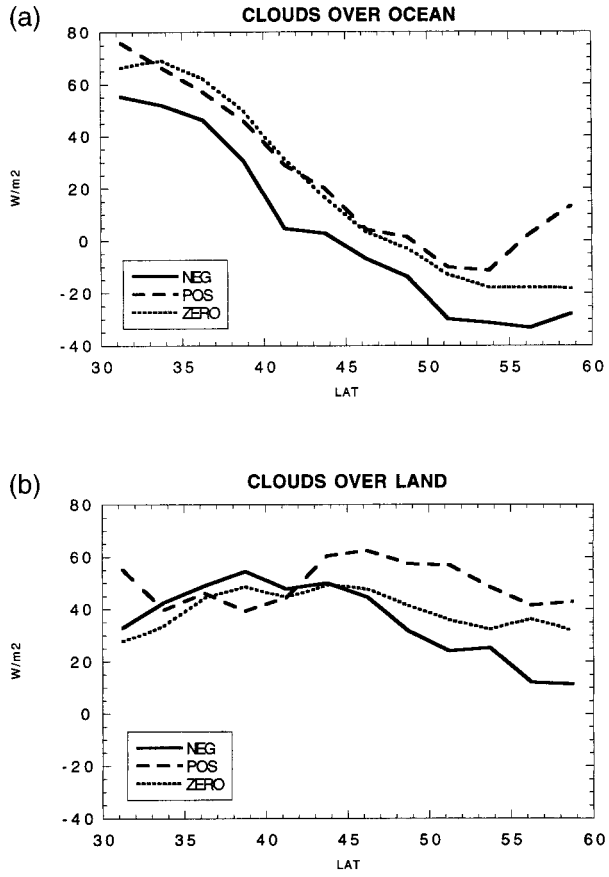

FIG. 17. As in Fig. 13 but for the net total (SW + LW) TOA flux.

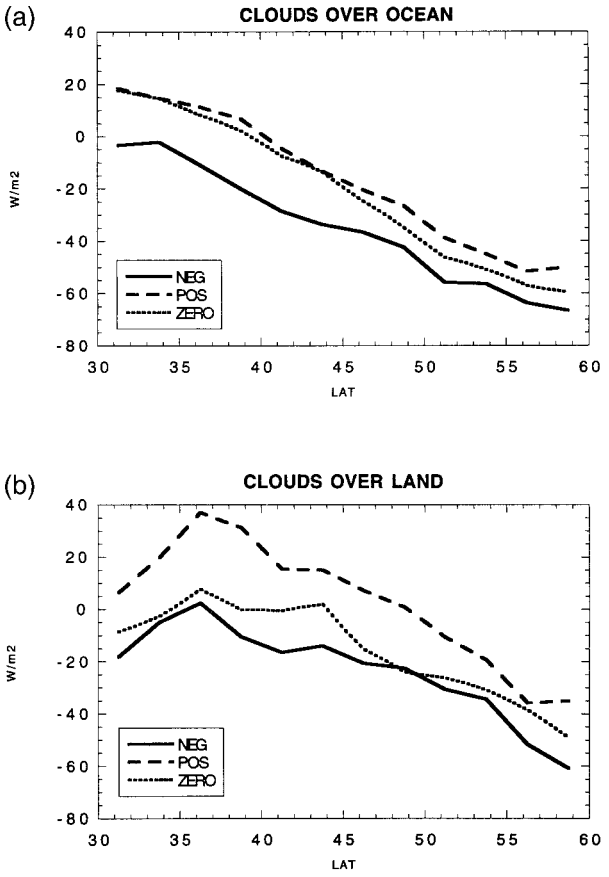

FIG. 18. As in Fig. 13 but for the net total (SW + LW) TOA flux in Apr 1990.

gime on the radiative balance can also be inferred from the results presented by Weaver and Ramanathan (1997), who correlated shortwave and longwave cloud radiative forcing to 500-mb vertical velocity. They found that more sunlight is reflected by the clouds and more heat is trapped by them in rising than in sinking motion regimes, and their plots also show that while these cooling and warming cloud effects nearly cancel each other in January, the excess cooling in the updraft regions is larger than the excess warming in July. The study of Weaver and Ramanathan (1997) also points to the fact that additional parameters, like vertical velocity and static stability, are important in understanding seasonal and regional variations of the radiative effects of clouds.

An attempt was made in this study to examine whether ''storm'' clouds damp or amplify the in-atmosphere energy balance of atmospheric eddies, by examining whether the passage of storm clouds tends to warm (cool) a warm (cold) atmosphere or to warm (cool) a cold (warm) atmosphere. Results of this attempt are not shown here, because uncertainty issues related to the use of TOVS temperature profiles and radiatively derived surface temperatures in zonal-mean statistics have not been explored enough. The preliminary results revealed both latitudinal and seasonal variations in the storm cloud effects on the in-atmosphere energy budget: the storm clouds tend to warm a cold atmosphere, particularly at summer high latitudes, but the opposite appeared to be true at winter high latitudes. This type of study will be the subject of future work, after a more thorough consideration of the appropriate data sources, data errors, and analysis techniques, with the objective to obtain cloud-induced vertical heating profile differences between dynamic regimes.

The results summarized above relate the midlatitude cloud type and radiative balance components to the atmospheric dynamics regime, as defined by the SLP anomaly. The results show large, primarily shortwave, radiative differences between regimes, caused by differing cloud cover and cloud type. This type of analysis provides a powerful tool that can be used to better understand the radiative balance differences between climate model simulations and satellite observations (e.g., Hahmann et al. 1995; DelGenio et al. 1996). Climate model outputs can be diagnosed in the same manner as the observational data, to document changes in cloud type and radiation between dynamic regimes. A comparison with the results of this study, then, is a first step

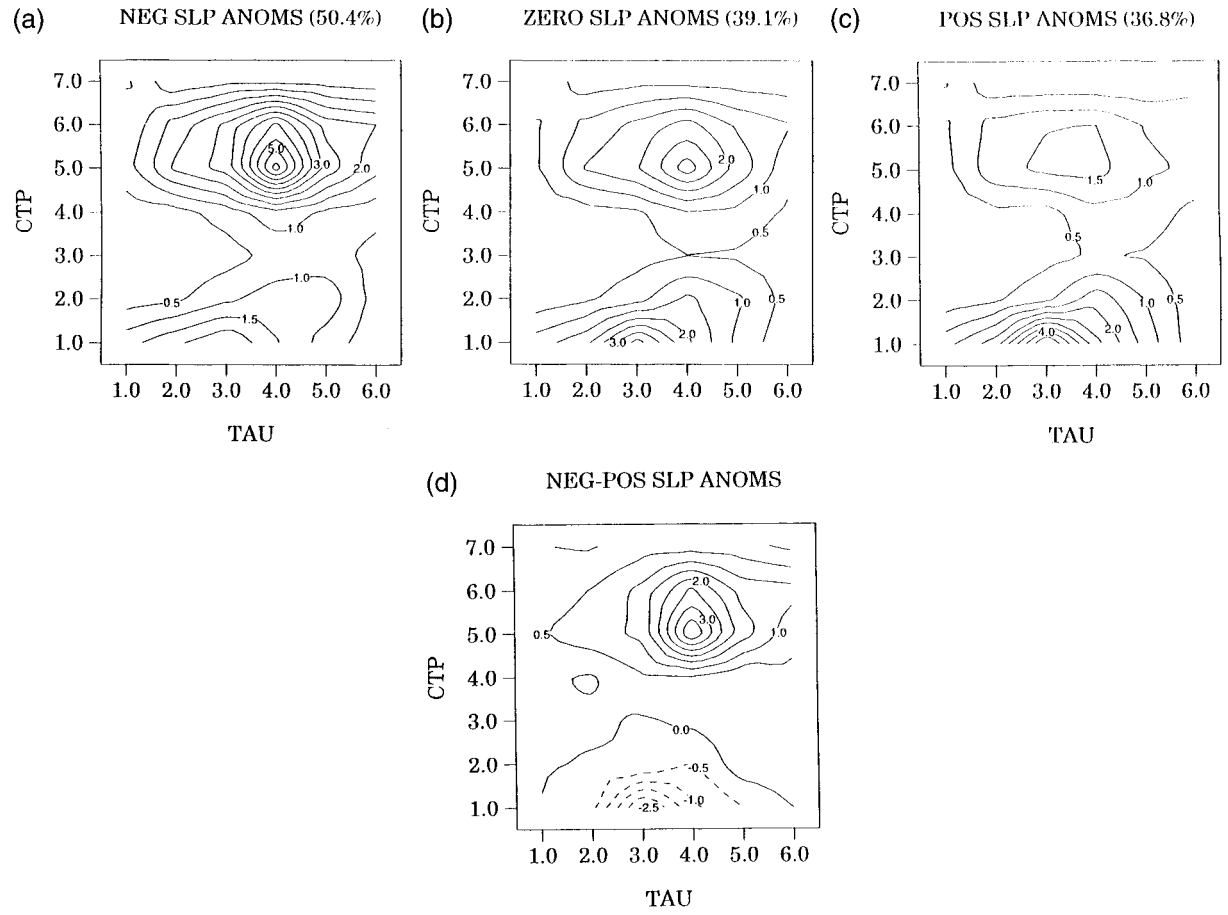

FIG. 19. As in Fig. 11 but for clouds over land from a Jul control simulation with the GISS GCM.

in an effort to attribute the model radiative discrepancies to particular dynamic processes, and could provide leads to potential deficiencies in the cloud formation schemes or the moisture transport mechanisms of the models. A preliminary result of such a comparison is shown in Fig. 19, where the distribution of cloud types in negative, positive, and zero SLPA regimes for land clouds from a July simulation with the GISS GCM are shown. Cloud properties in the model output are diagnosed from the top down, the way a satellite views clouds (e.g., DelGenio et al. 1996; Tselioudis et al. 1998). When compared to Fig. 12, the plot shows that the model underpredicts total cloud cover in all three regimes by amounts that are around 22%. The model produces a low cloud deck that becomes larger and optically thicker in the positive SLPA regime and a high cloud deck that becomes larger and optically thicker in the negative SLPA regime. Even though the amounts and optical thicknesses of the two cloud decks are both overpredicted, the model captures the direction of the cloud type changes between dynamic regimes. Where it fails is in capturing the background cloud field, as it severely underpredicts the middle and high thin clouds in all three dynamic regimes. Future work on this project will include more comparisons between model output and observational data with the use of additional definitions of dynamic regime and the inclusion of radiative budget comparisons in order to identify and correct those de-

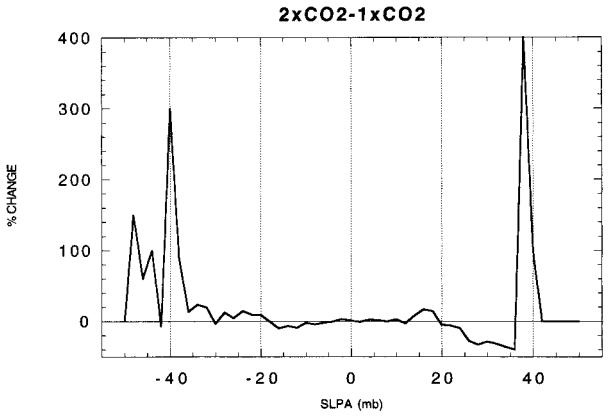

FIG. 20. Distribution of percent change in SLPA between a control and a doubled-CO_2 run with the GISS GCM, for the 30°–60°N lat zone.

ficiencies in the model schemes that are responsible for the radiative budget differences with the observations.

One climate implication of the changes in midlatitude cloud properties with atmospheric dynamics comes from the fact that most model simulations of greenhouse warming predict a decrease in the equator-to-pole temperature difference. Such a decrease would likely change the strength of the midlatitude dynamics, which in turn could effect the cloud and radiation fields. To investigate the changes with climate warming in the midlatitude SLP field, the frequency distribution of the January SLPA from an equilibrium doubled-CO_2 run with the GISS GCM was calculated, and the difference between this distribution and the same one from a current-climate January simulation with the model was calculated. This difference for the 30°–60°N lat zone is plotted in Fig. 20 as a percentage change between the current-climate and doubled-CO_2 runs. When examining this figure it is important to keep in mind that more than 95% of the data points in the two distributions lie within the −20–20-mb range (see also Fig. 1); this implies that any SLP-driven changes in the average cloud field and radiation budget between the current and the warmer climates will be determined by the pressure anomaly changes in the −20–20-mb range. Within this range the warmer climate shows a small decrease in the negative and a small increase in the positive SLPA populations, roughly of the order 10% each. A back of the envelope calculation using the TOA total flux differences between the positive and negative SLPA regimes from this study, suggests that changes of such magnitude in the SLPA distribution would introduce a TOA warming of 2–8 W m^{-2} in most seasons and a cooling of 1–3 W m^{-2} in the winter season.

A notable feature in Fig. 20 is the large increase with climate warming in the tail of the negative SLPA range. This implies a large increase with warming in the number of ''strong'' storms in the model atmosphere, which, due to the small number of cases involved, would have little effect on the radiation but may have strong impacts on the regional hydrology. This result happens despite the decrease in the meridional temperature gradient with climate warming and is in agreement with recent modeling studies by Carnell and Senior (1998), who found increases in the frequency of strong storm events in a doubled-CO_2 simulation with the HADCM2 Hadley Centre model.

The results of this study illustrate the potential for climate feedbacks from changes in the intensity of the dynamics–cloud–radiation cycle. Extensive modeling studies of those feedbacks, however, can be safely undertaken only after the climate models involved in such studies are thoroughly tested to establish whether they reproduce the observed relations between the atmospheric dynamics and cloud properties.

Acknowledgments. The authors wish to thank Diane Beuschel and Robert Kruckenberg for valuable help with software development and Anthony DelGenio for helpful comments and suggestions. This research was supported by the NASA Program on Global Radiation Data Analysis and Modeling managed by Dr. Robert J. Curran.

REFERENCES

Browning, K. A., 1994: *GEWEX Cloud System Study (GCSS): Science Plan.* IGPO Publication Series, Vol. 11, 62 pp.

Carnell, R. E., and C. A. Senior, 1998: Changes in mid-latitude variability due to increasing greenhouse gasses and sulphate aerosols. *Climate Dyn.,* **14,** 369–383.

Charlson, R. J., J. Langner, H. Rodhe, C. B. Leovy, and S. G. Warren, 1991: Perturbation of the Northern Hemisphere radiative balance by back-scattering from anthropogenic sulfate aerosols. *Tellus,* **43,** 152–163.

DelGenio, A. D., M.-S. Yao, W. Kovari, and K.-W. Lo, 1996: A prognostic cloud water parameterization for global climate models. *J. Climate,* **9,** 270–304.

Evans, M. S., D. Keyser, L. F. Bosart, and G. M. Lackmann, 1994: A satellite-derived classification scheme for rapid maritime cyclogenesis. *Mon. Wea. Rev.,* **122,** 1381–1416.

Hahmann, A. N., D. M. Ward, and R. E. Dickinson, 1995: Land surface temperature and radiative fluxes response of the NCAR CCM2/Biosphere–Atmosphere Transfer Scheme to modifications in the optical properties of clouds. *J. Geophys. Res.,* **100,** 23 239–23 252.

Hansen, J., G. Russel, D. Rind, P. Stone, A. Lacis, S. Lebedeff, R. Ruedy, and L. Travis, 1983: Efficient three-dimensional global models for climate studies: Models I and II. *Mon. Wea. Rev.,* **111,** 609–662.

Lacis, A. A., and V. Oinas, 1991: A description of the correlated k-distribution method for modeling non-gray gaseous absorption, thermal emission, and multiple scattering in vertically inhomogeneous atmospheres. *J. Geophys. Res.,* **96,** 9027–9063.

Lau, N.-C., and M. W. Crane, 1995: A satellite view of the synoptic scale organization of cloud properties in midlatitude and tropical circulation systems. *Mon. Wea. Rev.,* **123,** 1984–2006.

——, and ——, 1997: Comparing satellite and surface observations of cloud patterns in synoptic-scale circulation systems. *Mon. Wea. Rev.,* **125,** 3172–3189.

Liao, X., D. Rind, and W. B. Rossow, 1995: Comparison between SAGE II and ISCCP high-level clouds. Part II: Locating cloud tops. *J. Geophys. Res.,* **100,** 1137–1147.

Mishchenko, M. I., W. B. Rossow, A. Macke, and A. A. Lacis, 1996: Sensitivity of cirrus cloud albedo, bidirectional reflectance and optical thickness retrieval accuracy to ice particle shape. *J. Geophys. Res.,* **101,** 16 973–16 985.

Oort, A. H., 1983: Global atmospheric circulation statistics, 1958–1973. NOAA Professional Paper 14, NOAA Geophysical Fluid Dynamics Laboratory, U.S. Dept. of Commerce, Rockville, MD, 180 pp.

Rossow, W. B., and R. A. Schiffer, 1991: ISCCP cloud data products. *Bull. Amer. Meteor. Soc.,* **72,** 2–20.

——, and Y.-C. Zhang, 1995: Calculation of surface and top of atmosphere radiative fluxes from physical quantities based on ISCCP data sets. Part II: Validation and first results. *J. Geophys. Res.,* **100,** 1167–1197.

——, A. W. Walker, D. E. Beuschel, and M. D. Roiter, 1996: International Satellite Cloud Climatology Project (ISCCP) documentation of new cloud datasets. WMO/TD 737, World Climate Research Programme, Geneva, Switzerland, 115 pp.

Ryan, B. F., 1996: On the global variation of precipitating layer clouds. *Bull. Amer. Meteor. Soc.,* **77,** 53–70.

Toon, O. B., and J. B. Pollack, 1976: A global average model of atmospheric aerosols for radiative transfer calculations. *J. Appl. Meteor.,* **15,** 225–246.

Troup, A. J., and N. A. Streten, 1972: Satellite-observed Southern

Hemisphere cloud vortices in relation to conventional observations. *J. Appl. Meteor.,* **11,** 909–917.

Tselioudis, G., A. D. DelGenio, W. Kovari, and M.-S. Yao, 1998: Temperature dependence of low cloud optical thickness in the GISS GCM: Contributing mechanisms and climate implications. *J. Climate,* **11,** 3268–3281.

Wang, J., and W. B. Rossow, 1995: Determination of cloud vertical structure from upper-air observations. *J. Appl. Meteor.,* **34,** 2243–2258.

Weaver, C. P., and V. Ramanathan, 1996: The link between summertime cloud radiative forcing and extratropical cyclones in the North Pacific. *J. Climate,* **9,** 2093–2109.

——, and ——, 1997: Relationships between large-scale vertical velocity, static stability, and cloud radiative forcing over Northern Hemisphere extratropical oceans. *J. Climate,* **10,** 2871–2887.

Zhang, Y.-C., W. B. Rossow, and A. A. Lacis, 1995: Calculation of surface and top-of-atmosphere radiative fluxes from physical quantities based on ISCCP datasets. Part 1: Method and sensitivity to input data uncertainties. *J. Geophys. Res.,* **100,** 1149–1165.